ASCE

Analysis of Seismic Waves Propagating through an In Situ Stressed Rock Mass Using a Nonlinear Model

Tingting Liu[1]; Xinping Li[2]; Yun Zheng[3]; Fei Meng[4]; and Dongri Song[5]

Abstract: In situ stress is a significant characteristic of underground rock masses. This work extended the time-domain recursive method (TDRM) to study oblique wave attenuation across an in situ stressed joint wherein the normal and shear deformation behaviors were both treated nonlinearly. Employing the Barton–Bandis (B-B) and hyperbolic nonlinear (HN) slip models, equations were established for wave propagation across a rock mass under a combination of gravitational and tectonic stress. Then, the stress and displacement in the normal and shear directions were calculated under different in situ stresses for P- and S-wave incidence. The waveforms of the HN slip model and the Coulomb slip model were compared to investigate the differences therein and verify the wave propagation equation. Parametric studies were conducted to elucidate the influences of in situ stress, lateral pressure coefficient, angle of incidence, and amplitude of the incident wave. The results showed that the HN model depends on the stress history and shear stiffness degradation. The effect of the in situ stress on wave propagation depends not only on the gravitational and tectonic stresses but also on the direction of the particle vibration of the incident wave. **DOI: 10.1061/(ASCE)GM.1943-5622.0001621.**

Author keywords: Rock mass; In situ stress; Seismic attenuation; Time-domain recursive method; Displacement discontinuity model.

Introduction

One of the geological characteristics of underground rock masses is the occurrence of high in situ stress, which can be highly significant in terms of the safety and stability of underground engineering projects (Brown and Hoek 1978). In particular, in situ stress plays an important role in determining the strength and deformation characteristics of discontinuities (Hoek 1983; Pestman and Munster 1996; Utagawa et al. 1997; Korinets and Alehossein 2002; Zhao et al. 2008; Zhang 2010; Fairhurst 2003; Sebastian and Sitharam 2016; Cheng et al. 2017; Meng et al. 2019). When a blast or seismic wave encounters a discontinuity, the wave may undergo transmission, reflection, attenuation, and superposition with other waves. This can cause discontinuities to slip or experience closure, and reduces the strength of the rock mass (Aydan et al. 2010; Ning et al. 2011).

The velocity with which a wave propagates is closely related to the in situ stress, which in turn affects the dynamic response of the rock mass. The effect of in situ stress on the correlation between the velocity of P-waves and initial stress was studied using a variety of methods: uniaxial compressive tests (Kahraman 2001; Yasar and Erdogan 2004), ultrasonic wave tests (Chen and Xu 2016), quasi-static resonant column tests (Mohd-Nordin et al. 2014), and geostructural surveys (Pappalardo 2015). The results showed that the influence of in situ stress on elastic wave attenuation cannot be neglected. Tolstoy (1982) established dynamical equations for a prestressed solid subjected to overburden pressure and different stresses. Guz (2002) investigated elastic waves propagating in in situ stressed solids using a three-dimensional linear theory. Based on Biot's theory (Biot 1963), Sharma (2005) revealed the velocity and attenuation of waves propagating in anisotropic elastic solids subjected to in situ stress. Selim and Ahmed (2006) concluded that the propagation direction of a wave and the in situ stress in a medium both affect wave attenuation.

To consider the effect of vertical heterogeneity and initial stress, Singh et al. (2015) and Kumar et al. (2015) investigated SH-wave and Love-type wave propagation in composite layer, respectively. Shams (2016) studied wave propagation along the boundary between a half-space and a layer by considering the combined effect of in situ stress and finite deformation of the rock mass on the speed of Love waves.

In existing studies, the material is regarded as a continuum, and only the effect of in situ stress on the speed of waves was studied. The attenuation induced by discontinuities, e.g., joints, cracks, and faults, was ignored. However, the deformation of joints, e.g., slipping, opening up, and closure, will inevitably induce attenuation of the wave, energy dissipation, and delays in propagation time (Barton 1976; Bandis et al. 1983; Cook et al. 1992; Liu et al. 2000; Li et al. 2015; Misra and Marangos 2010; Zhou et al. 2017; Meng et al. 2018).

The displacement discontinuity method (DDM) has been widely used to investigate wave attenuation at joints of zero thickness

[1]Associate Professor, Key Laboratory of Roadway Bridge and Structure Engineering, Wuhan Univ. of Technology, Wuhan, Hubei 430070, PR China; Assistant Professor, State Key Laboratory of Geomechanics and Geotechnical Engineering, Institute of Rock and Soil Mechanics, Chinese Academy of Sciences, Wuhan, Hubei 430071, PR China. Email: ttliu@whut.edu.cn

[2]Professor, Key Laboratory of Roadway Bridge and Structure Engineering, Wuhan Univ. of Technology, Wuhan, Hubei 430070, PR China. Email: xinpingli@whut.edu.cn

[3]Assistant Professor, State Key Laboratory of Geomechanics and Geotechnical Engineering, Institute of Rock and Soil Mechanics, Chinese Academy of Sciences, Wuhan, Hubei 430071, PR China (corresponding author). Email: yzheng@whrsm.ac.cn

[4]Assistant Professor, State Key Laboratory of Geomechanics and Geotechnical Engineering, Institute of Rock and Soil Mechanics, Chinese Academy of Sciences, Wuhan, Hubei 430071, PR China; Assistant Professor, Faculty of Science, Engineering and Technology, Swinburne Univ. of Technology, Hawthorn, VIC 3122, Australia. Email: fmeng@swin.edu.au

[5]Associate Professor, Key Laboratory of Mountain Hazards and Earth Surface Process, Institute of Mountain Hazards and Environment, Chinese Academy of Sciences, Chengdu 610041, China. Email: drsong@imde.ac.cn

Note. This manuscript was submitted on April 4, 2019; approved on September 3, 2019; published online on January 2, 2020. Discussion period open until June 2, 2020; separate discussions must be submitted for individual papers. This paper is part of the ***International Journal of Geomechanics***, © ASCE, ISSN 1532-3641.

(Pyrak-Nolte et al. 1990; Zhao et al. 2006; Li et al. 2012). When a wave propagates across the joint, the DDM assumes that the displacement is discontinuous but the stress is continuous. The DDM also has been combined with the time-domain recursive method (TDRM) (Li et al. 2012), the method of characteristics (MC) (Zhao and Cai 2001, 2008), and the propagator matrix method (PMM) (Zhao et al. 2012) to study P- and S-wave propagation across single or sets of parallel joints described by different constitutive models (Zhu et al. 2011).

This paper proposes a new method which extends the TDRM to oblique wave propagation across in situ stressed rock masses under in situ stress, wherein the normal and shear deformation behaviors of the joint both are treated nonlinearly. Employing the Barton–Bandis (B-B) model and hyperbolic nonlinear (HN) slip models, equations were established for wave propagation across rock mass under a combination of gravitational and tectonic stress. Then the stress and displacement in the normal and shear directions were calculated under different in situ stresses for P- and S-wave incidence. Finally, parametric studies were conducted to study the role of in situ stress, lateral pressure coefficient, and the angle and amplitude of the incident wave.

Theoretical Model

Problem Description

Fig. 1 is a sketch of a jointed rock subject to in situ stress that contains a joint inclined at an arbitrary angle α_j. Two types of in situ stress are present: tectonic stress σ_{sh}, in the horizontal direction, and gravitational stress σ_{sv}, in the vertical direction. Fuchs and Müller (2001) established a map showing the tectonic stresses occurring around the world and pointed out that the Earth's continental crust permanently is in a state of frictional failure equilibrium and continually is being strengthened by a process of microfracture generation. Based on the principle of force equilibrium, the normal (σ_s) and shear (τ_s) stresses of a joint can be derived as follows:

$$\sigma_s = \sigma_{sv}\cos\alpha j + \sigma_{sh}\sin\alpha j$$
$$\tau_s = \sigma_{sv}\sin\alpha j + \sigma_{sh}\cos\alpha j \quad (1)$$

where α_j = angle of the joint in Fig. 1.

The lateral pressure coefficient k_v is defined as the ratio of the horizontal stress to vertical stress, i.e., $k_v = \sigma_{sh}/\sigma_{sv}$. Thus, Eq. (1) also can be written in the form

$$\sigma_s = \sigma_{sv}(\cos\alpha j + k_v \sin\alpha j)$$
$$\tau_s = \sigma_{sv}(\sin\alpha j + k_v \cos\alpha j) \quad (2)$$

Brown and Hoek (1978) statistically analyzed the stress in different regions of the world and found that the distribution of k_v is related closely to depth. Moreover, as depth increases, the value of k_v decreases. At a depth of 500 m, $k_v = 1.3$–3.5; at 2,500 m it decreases to 0.34–1.1. In the following calculations, the value of k_v is allowed to vary from 0.5 to 2.5.

Model of Joint Subject to In Situ Stress

When a plane wave propagates across a jointed rock mass at depth, the stresses acting on the joint includes dynamic and static in situ stress (Fan and Sun 2015). The joint will deform under the combined effect of the dynamic and in situ stresses. DDM has been widely used to study seismic wave propagation across a joint. In the DDM, a B-B model generally is used to describe the nonlinear elastic characteristic of normal mechanical behavior of the joint. When a plane wave propagates across the joint, the joint's normal stiffness varies with the current normal stress induced by the combined effect of the seismic wave and in situ stress.

In the B-B model, the relationship between the normal stress and closure can be expressed using a hyperbolic equation [Fig. 2(a)]

$$d_n = \frac{\sigma}{k_{ni} + \sigma/d_{\max}} \quad (3)$$

where k_{ni} = initial normal stiffness; σ = normal stress acting on joint; and d_n and $d_{\max}$ = normal closure value and its maximum allowable value, respectively. The normal stiffness increases when the normal stress increases [Fig. 2(a)]. That is, wave propagation is dependent upon the in situ stress. The normal deformation of the joint includes contributions from the static closure d_s (induced by the in situ stress) and the dynamic closure d_w (caused by the stress wave).

For the shear deformation of the joint, the hyperbolic nonlinear slip model proposed by Kulhawy (1975) is extended to describe the relationship between the shear deformation and shear stress in the prepeak range. That is

$$\tau_n = \frac{u}{m + nu} \quad (4)$$

where u = joint shear displacement; τ_n = shear stress acting on joint; $m = 1/k_{si}$ = constant, where k_{si} = initial shear stiffness

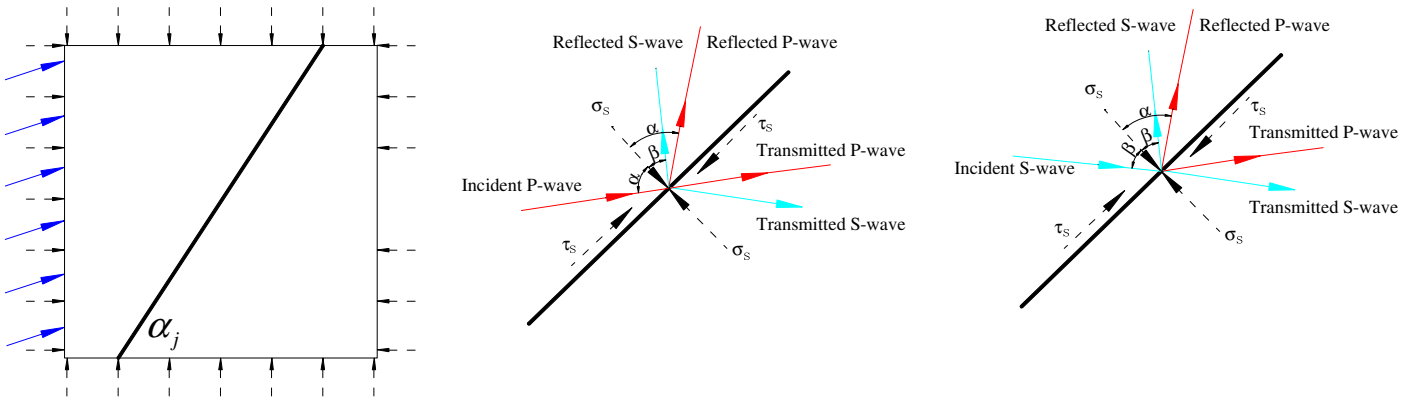

Fig. 1. In situ stress in a rock mass containing a joint with an arbitrary angle of inclination, α_j.

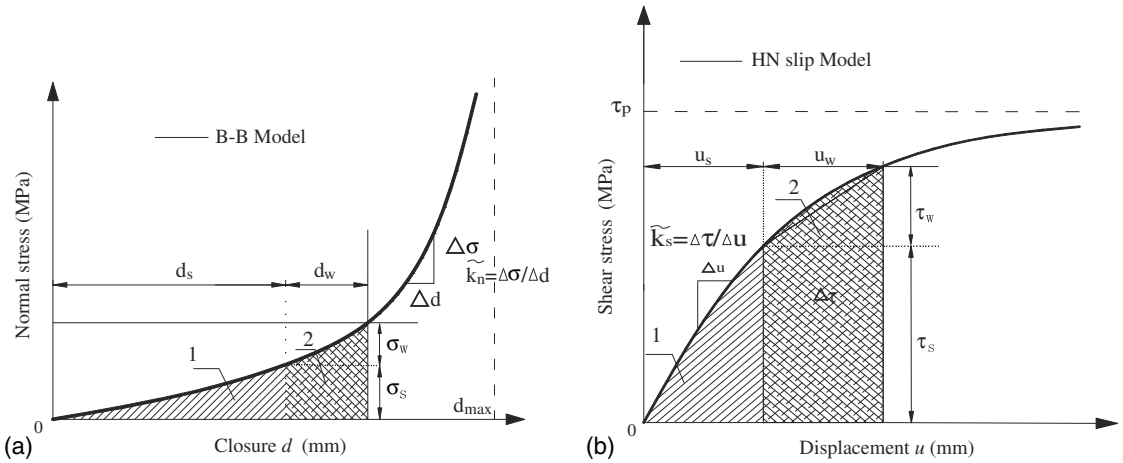

Fig. 2. Mechanical behavior of joint considering in situ stress: (a) B-B model for normal; and (b) HN slip mode for shear.

obtained using Eq. (5); and n = constant equal to reciprocal of limiting value of τ.

It is clear that the current shear stiffness k_s at any level of shear and normal stress varies with τ and this can be described via the expression

$$k_s = \frac{\Delta\tau}{\Delta u} = K_j(\sigma)^{n_i}\left(1 - \frac{\tau R_f}{c + \sigma\tan\varphi}\right) = k_{si}\left(1 - \frac{\tau R_f}{c + \sigma\tan\varphi}\right) \tag{5}$$

where K_j and n_i = joint shear stiffness number and stiffness exponent, respectively; τ and σ = current shear stress and normal stress of joint, respectively; R_f = failure ratio (equal to ratio of τ to τ_{ult}); and c and φ = cohesion and friction angle of joint, respectively. The HN model is stress-dependent and can be used to evaluate the shear stiffness under any level of shear stress and normal stress (Kulhawy 1975). For a given normal stress, the shear stiffness decreases with increasing shear stress. When a wave propagates across the joint, the shear deformation is composed of two parts, namely, the static deformation u_s induced by the in situ stress, and dynamic shear deformation u_w caused by the stress wave (Fig. 2).

Wave Propagation Equation

The time-domain recursive method proposed by Li et al. (2012) was extended here to investigate the role of in situ stress on wave attenuation. The HN and B-B models were used to describe the shear and compressive behavior of the joint, respectively. The basic equations used in the TDRM were derived using Snell's law and assuming continuous boundary conditions. By balancing the momentum acting on the wave fronts and the interaction between the stress wave and joint, the stress induced by the stress wave on the two sides of the joint could be expressed as (Li et al. 2012; Li 2013) follows:

Left-hand side

$$\begin{aligned}\sigma_w^- &= z_p\cos 2\beta v_{Ip} + z_s\sin 2\beta v_{Rp} - z_s\sin 2\beta v_{Rs}\\ \tau_w^- &= (v_{Ip} - v_{Rp})z_p\sin 2\beta\tan\beta/\tan\alpha - z_s\cos 2\beta v_{Rs}\end{aligned} \quad \text{for P-wave incidence} \tag{6}$$

$$\begin{aligned}\sigma_w^- &= z_s\sin 2\beta v_{Is} - z_s\sin 2\beta v_{Rs} + z_p\cos 2\beta v_{Rp}\\ \tau_w^- &= -z_s\cos 2\beta(v_{Is} + v_{Rs}) - v_{Rp}z_p\sin 2\beta\tan\beta/\tan\alpha\end{aligned} \quad \text{for S-wave incidence} \tag{7}$$

Right-hand side

$$\begin{aligned}\sigma_w^+ &= z_p\cos 2\beta v_{Tp} + z_s\sin 2\beta v_{Ts}\\ \tau_w^+ &= v_{Tp}z_p\sin 2\beta\tan\beta/\tan\alpha - z_s\cos 2\beta v_{Ts}\end{aligned} \quad \text{for P- or S-wave incidence} \tag{8}$$

where σ_w^m and τ_w^m = normal and shear stresses on each side of joint, respectively, where $m = -, +$; v_{Ip} and v_{Is} = particle velocities of P-wave incidence and S-wave incidence, respectively; v_{Tp} and v_{Rp} = particle velocities of transmitted and reflected P-waves, respectively, v_{Ts} and v_{Rs} = particle velocities of transmitted and reflected S-waves, respectively; and $z_p = \rho c_p$ and $z_s = \rho c_s$ = wave impedance of P- and S-waves, respectively, where ρ = rock density, and c_p and c_s = P-wave velocity and S-wave velocity of intact rock, respectively.

The particle velocity was determined by the dynamic stress when a plane wave propagates through a joint. Considering the intact rock and joint to be linear and nonlinear elastic materials,

respectively, the normal and tangential components of the velocities on the left- and right-hand sides of the joint can be derived, giving

$$\begin{aligned} v_n^- &= \cos\alpha(v_{Ip} - v_{Rp}) + \sin\beta v_{Rs} \\ v_\tau^- &= \sin\alpha(v_{Rp} + v_{Ip}) + \cos\beta v_{Rs} \end{aligned} \quad \text{for P-wave incidence} \tag{9}$$

$$\begin{aligned} v_n^- &= \sin\beta(v_{Is} + v_{Rs}) - \cos\alpha v_{Rp} \\ v_\tau^- &= \cos\beta(v_{Rs} - v_{Is}) + v_{Rp}\sin\alpha \end{aligned} \quad \text{for S-wave incidence} \tag{10}$$

$$\begin{aligned} v_n^+ &= \cos\alpha v_{Tp}\sin\beta v_{Ts} \\ v_\tau^+ &= \sin\alpha v_{Tp} - \cos\beta v_{Ts} \end{aligned} \quad \text{for P- or S-wave incidence} \tag{11}$$

where v_n^- and v_n^+ = normal velocities on left- and right-hand sides of joint, respectively; and v_τ^- and v_τ^+ = tangential velocities on left and right sides of the joint, respectively. Based on stress-continuous and displacement-discontinuous boundary conditions, the stresses and displacements of the joint sides satisfy the following equations:

$$\begin{aligned} \sigma &= \sigma^- = \sigma^+ = \sigma_s + \sigma_w \\ \tau &= \tau^- = \tau^+ = \tau_s + \tau_w \end{aligned} \tag{12}$$

$$\begin{aligned} u_n^- - u_n^+ &= \frac{\sigma}{k_{ni} + (\sigma/d_{\max})} = \frac{\sigma}{\tilde{k}_n} \\ u_\tau^- - u_\tau^+ &= \Delta u_\tau = \frac{\tau}{\tilde{k}_s} \end{aligned} \quad \text{for } |\tau_w + \tau_s| < \tau_p \tag{13}$$

$$\begin{aligned} &u_n^- - u_n^+ = \frac{\sigma}{k_{ni} + (\sigma/d_{\max})} = \frac{\sigma}{\tilde{k}_n} \\ &\tau = \pm\tau_p \\ &\tau_p = \sigma\tan\varphi = (\sigma_s + \sigma_w)\tan\varphi = \tau_{p0} + \sigma_w\tan\varphi \end{aligned} \quad \text{for } |\tau_w + \tau_s| < \tau_p \tag{14}$$

where $\tau_{p0} = \sigma_s \tan\varphi$ = static shear strength under in situ stress conditions; and $\tilde{k}_n$ and $\tilde{k}_s$ = generalized normal stiffness and shear stiffness of joint, respectively, and are given by

$$\begin{aligned} \tilde{k}_s &= K_j\sigma^{nj}\left(1 - \frac{\tau R_f}{\tau_0}\right) = K_j(\sigma_s + \sigma_w)^{n_i}\left(1 - \frac{(\tau_s + \tau_w)R_f}{\tau_0}\right) \\ \tilde{k}_n &= \frac{(k_{ni} + \sigma/d_{\max})^2}{k_{ni}} = \frac{[k_{ni} + (\sigma_s + \sigma_w)/d_{\max}]^2}{k_{ni}} \end{aligned} \tag{15}$$

Differentiating Eqs. (13) and (14) with respect to time, t, yields

$$\begin{aligned} v_n^-(i) - v_n^+(i) &= \frac{1}{\tilde{k}_n}\frac{\sigma_w(i+1) - \sigma_w(i)}{\Delta t} \\ v_\tau^-(i) - v_\tau^+(i) &= \frac{1}{\tilde{k}_s}\frac{\partial\tau}{\partial t} = \frac{1}{\tilde{k}_s}\frac{\tau_w(i+1) - \tau_w(i)}{\Delta t} \end{aligned} \quad \text{for } |\tau_w + \tau_s| < \tau_p \tag{16}$$

$$\begin{aligned} &v_\tau^-(i) - v_\tau^+(i) = \frac{1}{\tilde{k}_s}\frac{\partial\tau}{\partial t} = \frac{1}{\tilde{k}_s}\frac{\tau_w(i+1) - \tau_w(i)}{\Delta t} \\ &|\tau_w(i) + \tau_s| = \tau_{p0} + \sigma_w(i)\tan\varphi \end{aligned} \quad \text{for } |\tau_w + \tau_s| \geq \tau_p \tag{17}$$

where Δt = small time interval.

When the shear stress reaches the shear strength of the joint, slipping will occur. Therefore, when an incident P- or S-wave impinges upon a joint, it may be subjected to two modes of shear deformation: an elastic deformation mode, or a plastic slip mode. In this analysis, we categorize the behavior into four distinct cases, as follows:

1. An incident P-wave with $|\tau_w + \tau_s| < \tau_p$

   We substitute Eqs. (6) and (8) into Eq. (12) and Eqs. (9) and (11) into Eq. (16), and combine the results with Eq. (15) to derive an equation for the propagation of the wave across the joint. The results are expressed in matrix form

$$\begin{bmatrix} v_{Rp}(i) \\ v_{Rs}(i) \end{bmatrix} = A^{-1}Bv_{Ip}(i) + A^{-1}C\begin{bmatrix} v_{Tp}(i) \\ v_{Ts}(i) \end{bmatrix} \tag{18}$$

$$\begin{aligned} \begin{bmatrix} v_{Tp}(i+1) \\ v_{Ts}(i+1) \end{bmatrix} &= G^{-1}Dv_{Ip}(i) + G^{-1}E\begin{bmatrix} v_{Rp}(i) \\ v_{Rs}(i) \end{bmatrix} \\ &\quad + G^{-1}F\begin{bmatrix} v_{Tp}(i) \\ v_{Ts}(i) \end{bmatrix} \end{aligned} \tag{19}$$

where A–G are given by

$$A = \begin{bmatrix} z_P\cos 2\beta \\ z_P\sin 2\beta\tan\beta\cot\alpha \end{bmatrix}$$

$$B = \begin{bmatrix} z_P\cos 2\beta & -z_S\sin 2\beta \\ -z_P\sin 2\beta\tan\beta\cot\alpha & -z_S\cos 2\beta \end{bmatrix}$$

$$C = \begin{bmatrix} z_P\cos 2\beta & z_S\sin 2\beta \\ z_P\sin 2\beta\tan\beta\tan\alpha & -z_S\cos 2\beta \end{bmatrix}$$

$$D = \begin{bmatrix} \tilde{k}_n\Delta t\cos\alpha \\ \tilde{k}_s\Delta t\sin\alpha \end{bmatrix}$$

$$E = \begin{bmatrix} \tilde{k}_n\Delta t\cos\alpha & \tilde{k}_n\Delta t\sin\beta \\ \tilde{k}_s\Delta t\sin\alpha & \tilde{k}_s\Delta t\cos\beta \end{bmatrix}$$

$$F = \begin{bmatrix} -\tilde{k}_n\Delta t\cos\alpha + z_P\cos 2\beta & -\tilde{k}_n\Delta t\sin\beta + z_S\sin 2\beta \\ -\tilde{k}_s\Delta t\sin\alpha + z_P\sin 2\beta\tan\beta\cot\alpha & \tilde{k}_s\Delta t\cos\beta - \tilde{k}_s\cos 2\beta \end{bmatrix}$$

$$G = \begin{bmatrix} z_P\cos 2\beta & z_S\sin 2\beta \\ z_P\sin 2\beta\tan\beta\cot\alpha & -z_s\cos 2\beta \end{bmatrix}$$

2. An incident P-wave with $|\tau_w + \tau_s| \geq \tau_p$

   Following the same procedure, the propagation of the wave in this case can be written

$$\begin{bmatrix} v_{Rp}(i) \\ v_{Rs}(i) \end{bmatrix} = A^{-1}Bv_{ip}(i) + A^{-1}C\begin{bmatrix} v_{Tp}(i) \\ v_{Ts}(i) \end{bmatrix} \tag{20}$$

$$\begin{bmatrix} v_{Tp}(i+1) \\ v_{Ts}(i+1) \end{bmatrix} = G^{-1}Dv_{Ip}(i) + G^{-1}E\begin{bmatrix} v_{Rp}(i) \\ v_{Rs}(i) \end{bmatrix} + G^{-1}F\begin{bmatrix} v_{Tp}(i) \\ v_{Ts}(i) \end{bmatrix} + G^{-1}H(\tau_{ps} \mp \tau_s) \quad (21)$$

where A–H take the forms

$$A = \begin{bmatrix} z_P \cos 2\beta \\ z_P \sin 2\beta \tan\beta \cot\alpha \end{bmatrix}$$

$$B = \begin{bmatrix} z_P \cos 2\beta & -z_S \sin 2\beta \\ -z_P \sin 2\beta \tan\beta \cot\alpha & -z_S \cos 2\beta \end{bmatrix}$$

$$C = \begin{bmatrix} z_P \cos 2\beta & z_S \sin 2\beta \\ 0 & 0 \end{bmatrix}$$

$$D = \begin{bmatrix} \tilde{k}_n \Delta t \cos\alpha \\ 0 \end{bmatrix}$$

$$E = \begin{bmatrix} -\tilde{k}_n \Delta t \cos\alpha & \tilde{k}_n \Delta t \sin\beta \\ 0 & 0 \end{bmatrix}$$

$$F = \begin{bmatrix} -k_n \Delta t \cos\alpha + z_P \cos 2\beta & -k_n \Delta t \sin\beta + z_S \sin 2\beta \\ 0 & 0 \end{bmatrix}$$

$$G = \begin{bmatrix} z_P \cos 2\beta & z_P \sin 2\beta \tan\beta \cot\alpha \\ z_P \sin 2\beta \tan\beta \cot\alpha \mp z_S \sin 2\beta & -z_s \cos 2\beta \mp z_s \sin 2\beta \tan\varphi \end{bmatrix}$$

$$H = \begin{Bmatrix} 0 \\ \pm 1 \end{Bmatrix}$$

The symbol $\pm$ in H represents the two different possible sliding directions under the action of the shear stress induced by the combined effect of the stress wave and in situ stress.

3. An incident S-wave with $|\tau_w + \tau_s| < \tau_p$

   Substituting Eqs. (7) and (8) into Eq. (12) and Eqs. (10) and (11) into Eq. (16), and combining the results with Eq. (15), the equation for the wave propagation across the jointed rock mass can be derived in the same form as Eqs. (18) and (19) (Li 2013), with minor changes. Namely, $v_{Ip}(i)$ is replaced by $v_{Is}(i)$, and A and D are changed to

$$A = \begin{bmatrix} z_s \sin 2\beta \\ -z_s \cos 2\beta \end{bmatrix} \quad \text{and} \quad D = \begin{bmatrix} k_n \Delta t \sin\beta \\ -k_S \Delta t \cos\beta \end{bmatrix}$$

   The other parameters are the same as those in Eqs. (18) and (19).

4. An incident S-wave with $|\tau_w + \tau_s| \geq \tau_p$

   Following the same procedure, the resulting expressions are found to be the same as those given in Eqs. (20) and (21) but with $v_{Ip}(i)$ replaced by $v_{Is}(i)$, and

$$A = \begin{bmatrix} z_s \sin 2\beta \\ -z_s \cos 2\beta \end{bmatrix} \quad \text{and} \quad D = \begin{bmatrix} k_n \Delta t \sin\beta \\ 0 \end{bmatrix}$$

   The other parameters are the same as previously.

Special Case and Comparison

Comparison of Different Joint Models

Unlike their linear counterparts, nonlinear elastic models depend on the stress, and the stiffness of the joint varies as the stress wave propagates across it. The propagation of waves across joints with nonlinear normal behavior has been systematically studied (Li 2013; Zhao et al. 2006). The present paper focused mainly on the effect of nonlinear shear behavior and in situ stress on wave attenuation. Therefore, in this section the propagation of waves across joints subject to different in situ stresses was investigated using three different types of joint model. The first type is a linear model wherein a linearly elastic model was used to describe both the normal and shear behaviors of the joint. The second model is referred to as the Nonlinear 1 model. Herein, the B-B model and Mohr–Coulomb slip model were used to describe the joint normal and shear behaviors, respectively. The third model is referred to as the Nonlinear 2 model. In this model, the same model is used in the normal direction as in Nonlinear 1 model, whereas the model in the shear direction is changed to the HN slip model.

In the following cases, the density of the intact rock was assumed to be 2,650 kg/m^3, and the P-wave velocity (c_p) and shear wave velocity (c_s) were taken to be 6,218 and 3,836 m/s, respectively. For the Nonlinear 2 model, the initial normal stiffness (k_{ni}) was taken to be 3.5 GPa/m and $d_{\max} = 1$ mm. The joint shear stiffness number (K_j) was 3.88 GPa/m. The stiffness exponent (n_i) and failure ratio (R_f) were 0.000725 and 0.810, respectively. For the Nonlinear 1 model, the parameters for the normal behavior were same as those in the Nonlinear 2 model, whereas the shear stiffness (k_s) was set equal to k_{ni}. For the linear model, the normal and shear stiffnesses both were set to 3.5 GPa/m. The in situ gravitational stress (σ_{sv}) was 0.5 MPa and the lateral pressure coefficient (k_v) was 1. The joint angle (α_j) was taken to be 30°. The incident P-wave and S-wave both were assumed to have half-cycle sinusoidal waveforms with a frequency and amplitude of 50 Hz and 0.1 m/s, respectively.

Fig. 3 shows the results obtained using the three models for the transmitted and reflected P-waves for two angles of incidence: 0° and 30°. When a P-wave is incident normally on the joint [Fig. 3(a)], the transmitted and reflected P-waves obtained using the Nonlinear 1 and 2 models are almost exactly the same. However, when the wave is incident obliquely [Fig. 3(b)], the transmitted P-wave amplitude is larger in the Nonlinear 1 model than that in the Nonlinear 2 model. For both of the angles of incidence, the transmitted P-wave amplitude obtained from the linear model is the smallest. This is because the transmitted wave amplitude increases when the joint stiffness increases (Zhao and Cai 2001; Li et al. 2012). For the Nonlinear 1 and 2 models, the joint normal stiffness increases as the normal stress increases. On the other hand, for the linear model, the normal stiffness is constant. The shear stiffness also increases when the normal stress increases or the shear stress decreases.

Fig. 4 illustrates the results obtained for transmitted and reflected S-waves for different angles of incidence and vertical stresses. When the S-wave is incident normally and $\sigma_{sv} =$ 2.5 MPa [Fig. 4(a)], the reflected and transmitted S-waves calculated using the linear and Nonlinear 1 models are almost identical.

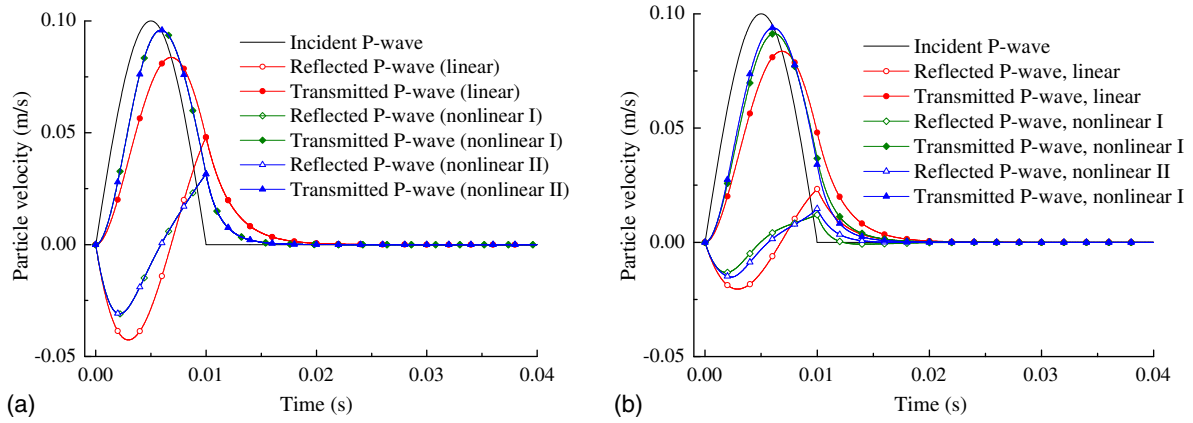

Fig. 3. Transmission and reflection of P-waves propagating across the three types of joint for two different angles of incidence: (a) normal incidence ($\alpha = 0°$); and (b) oblique incidence ($\alpha = 30°$).

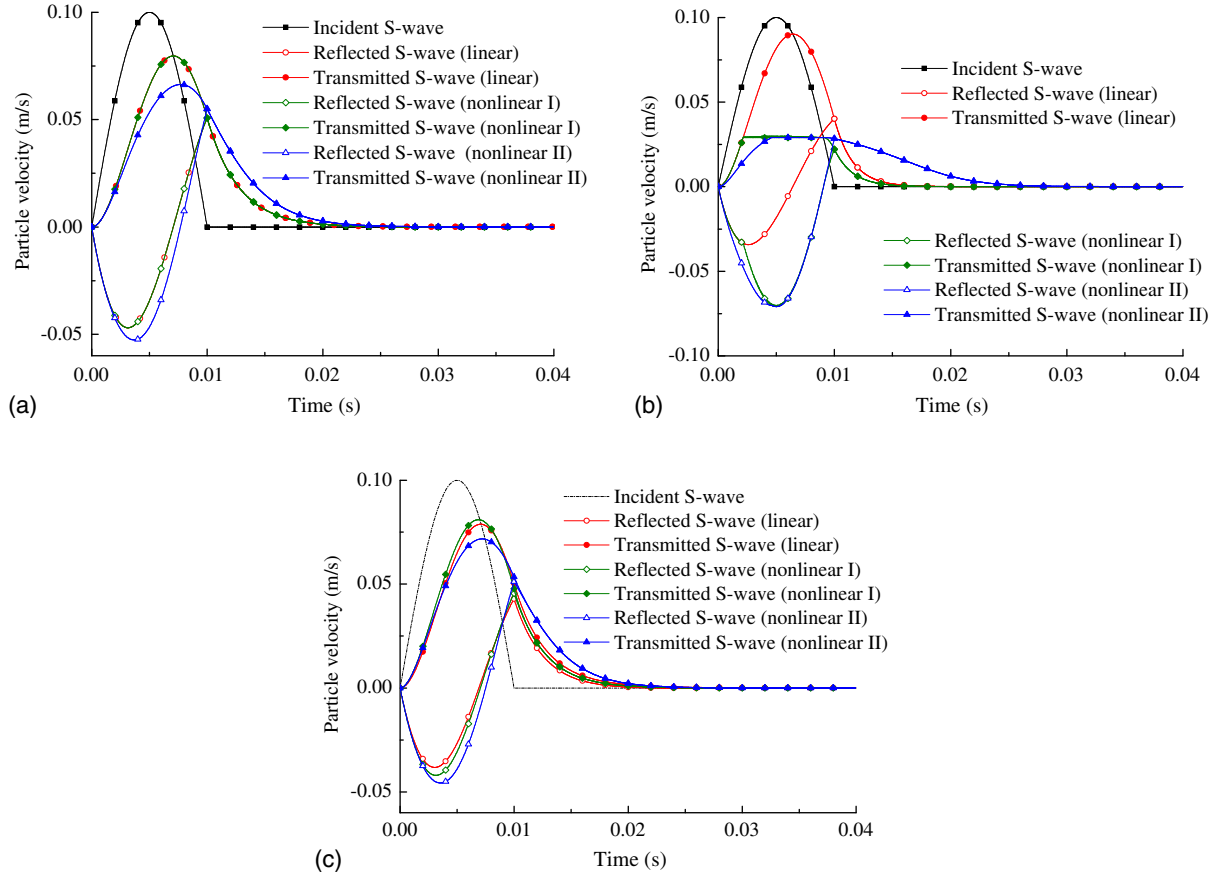

Fig. 4. Transmitted and reflected S-waves for an incident S-wave: (a) normal incidence with $\sigma_{sv} = 2.5$ MPa; (b) normal incidence with $\sigma_{sv} = 0.5$ MPa; and (c) oblique incidence with $\sigma_{sv} = 2.5$ MPa and $\beta = 30°$.

Furthermore, the amplitude of the transmitted wave obtained using the Nonlinear 2 model is the lowest. When the value of σ_{sv} is decreased to 0.5 MPa [Fig. 4(b)], the amplitudes of the reflected and transmitted S-waves calculated using the Nonlinear 1 model are equal to those calculated using the Nonlinear 2 model. The transmitted S-waves calculated using these two nonlinear models are cut off, which indicates that the shear stress reaches the shear strength of the joint and so slipping occurs.

When the S-wave is incident on the joint obliquely [Fig. 4(c)], the transmitted waves calculated using the three joint models are all different, and they have different amplitudes: 0.071, 0.078, and 0.081 m/s. These differences are caused by the differences in the stiffness and shear strength, which is affected by the normal and shear stresses. During the propagation of the wave, the shear stiffness of the joint changes in the different models according to the following rules:

1. For the linear model, the shear stiffness remains unchanged;
2. For the Nonlinear 1 model, the shear stiffness remains unchanged until slip occurs;
3. For the Nonlinear 2 model, the shear stiffness decreases when the shear stress increases or the normal stress decreases.

The normal stiffness of the joint changes in the different models according to the following rules:

1. For the linear model, the normal stiffness remains unchanged;
2. For the Nonlinear 1 model, the normal stiffness increases when the normal stress increases;
3. For the Nonlinear 2 model, the normal stiffness increases when the normal stress increases.

The results indicate that the way a wave propagates through a joint is closely related to the joint model used and the incident angle. Compared with the other two models, the effect on wave propagation of the in situ stress and mechanical behavior of the joint can be taken into account using the Nonlinear 2 model.

Effect of In Situ Stress

In this section, the Nonlinear 2 model was used to study waves propagating at right angles to a joint subjected to different in situ stresses. The waveforms thus obtained for P-waves subjected to two different values of in situ stress, and the relationship between the closure and stress on the joint, are shown in Fig. 5.

Although the mechanical behavior is the same, the transmitted wave amplitude is larger when σ_{sv} is 2.5 MPa than when it is 0.5 MPa [Fig. 5(a)]. Fig. 5(b) demonstrates that the initial closures caused by in situ stresses of 0.5 and 2.5 MPa are 0.31 mm (Stage PO-PA,) and 0.65 mm (Stage PO-PC), respectively. When a P-wave of amplitude 0.1 m/s is subsequently incident normally at the joint, additional displacement occurs. The dynamic closures caused by the stress wave are 0.3 mm (Stage PA-PB) and 0.1 mm (Stage PC-PD) when $\sigma_{sv} = 0.5$ and 2.5 MPa, respectively. These results show that the in situ stress plays an important role in the initial closure of the joint and the stress state closely associated with wave attenuation. In other words, the in situ stress is a significant factor affecting the dynamic response of the underground rock mass.

The direction of the shear stress caused by an S-wave may be opposite to that of the in situ shear stress. Therefore, to better understand the effect of in situ stress, S-waves with amplitudes of 0.1 and −0.1 m/s were applied to the model and the transmitted wave, reflected wave, shear deformation, and shear stress were calculated. Here, we use the symbols + and − to represent the direction of vibration caused by the S-wave, consistent with the work of Li et al. (2013). The in situ shear stresses of the joint subjected to σ_{sv} values of 0.5 and 2.5 MPa are −0.18 and −0.9 MPa, respectively. The corresponding in situ normal stresses are 0.68 and 3.4 MPa, respectively. When the S-wave has a positive amplitude (i.e., a + waveform), the dynamic shear stress has a negative amplitude (i.e., a − waveform), which is calculated using Eq. (7). This means that the direction of deformation caused by the S-wave is the same as that of the initial shear deformation caused by the in situ shear stress. The shear deformations when $\sigma_{sv} = 0.5$ and 2.5 MPa correspond to SO–SA1 and SO–SB1, respectively [Fig. 6(b)].

The initial shear displacements caused by in situ stresses of 0.5 and 2.5 MPa are 0.06 mm (Stage SO–SA1) and 0.27 mm (Stage SO–SB1), respectively. When the sinusoidal S-wave of amplitude 0.1 m/s is normally incident on the joint subjected to $\sigma_{sv} = 0.5$ MPa, the shear deformation can be divided into three parts as wave propagation proceeds. First, as the incident vibration velocity increases to the critical value (v_{cri}), at which point the total shear stress ($\tau_w + \tau_s$) is equal to the shear strength, the shear deformation increases along the direction of the initial shear deformation, which corresponds to SA1–SA2 [Fig. 6(b)]. When the incident vibration velocity increases to its peak value and decreases to v_{cri}, slipping occurs and the shear deformation increases dramatically, whereas the shear stress remains unchanged; this corresponds to SA2–SA3. As the incident vibration velocity decreases to 0, the shear deformation decreases, which corresponds to SA3–SA4.

When $\sigma_{sv} = 2.5$ MPa, slipping does not occur because the total shear stress is smaller than the shear strength. The shear deformation of the joint therefore corresponds to SB1–SB2–SB1 as the wave propagates. As a result, the transmitted S-wave when $\sigma_{sv} = 0.5$ MPa is cut off, whereas that when $\sigma_{sv} = 2.5$ MPa is not. The results also indicate that the joint is more likely to slip when the in situ stress is lower.

An S-wave with an amplitude of −0.1 m/s [Figs. 6(c and d)] was considered. The direction of the deformation caused by the vibration is opposite to that of the initial shear deformation induced by the in situ shear stress. The shear deformations when $\sigma_{sv} = 0.5$ and 2.5 MPa correspond to SO–SC1 and SO–SD1, respectively (which are the same as SO–SA1 and SO–SB1 in Fig. 6(b), respectively) [Fig. 6(d)]. The shear deformation induced by the S-wave is in the opposite direction to the initial shear displacement. The paths

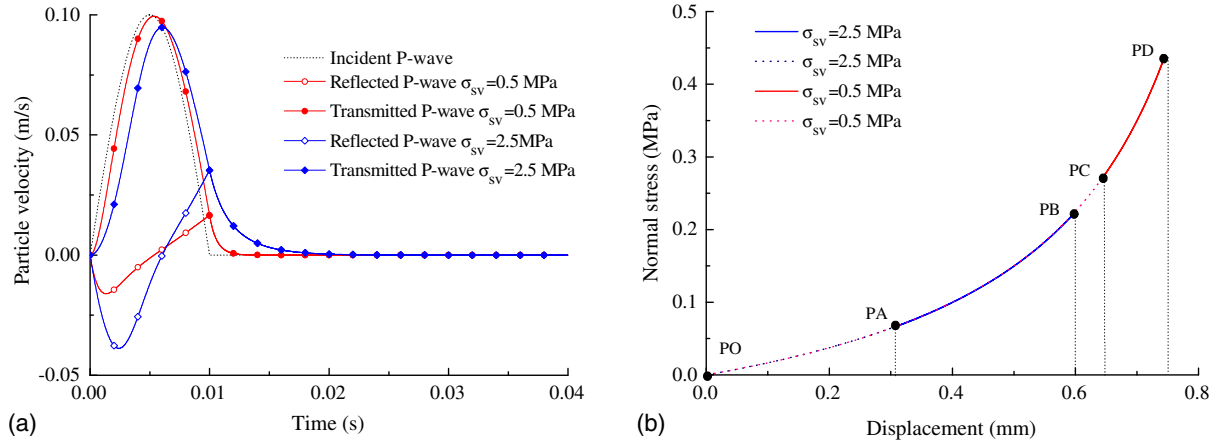

Fig. 5. Effect of in situ stress on P-wave propagation normally and the joint relative normal deformation: (a) transmitted and reflected P-waves; and (b) closure and stress under different in-situ stress.

Int. J. Geomech., 2020, 20(3): 04020002

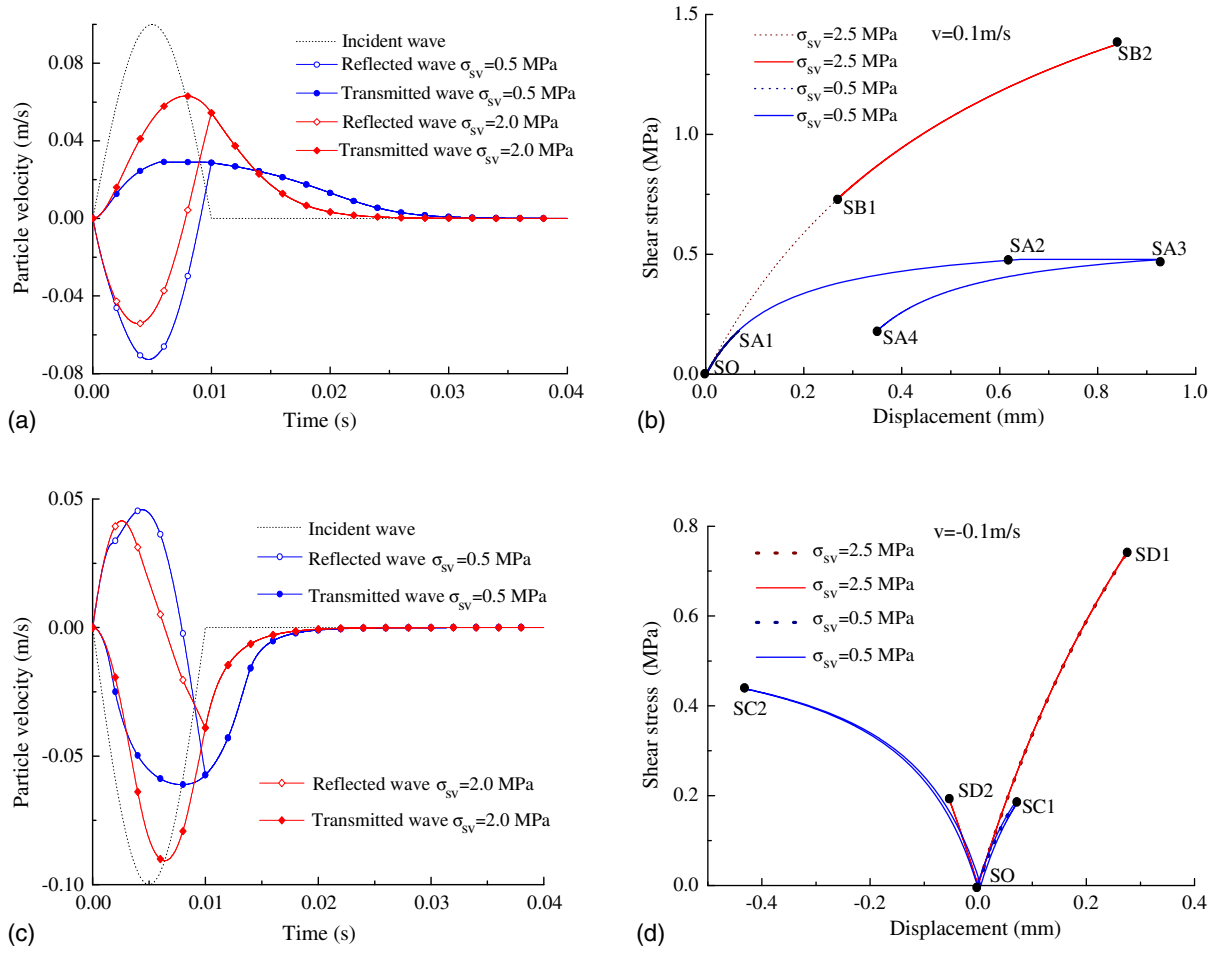

Fig. 6. Effect of different in situ stresses on normally propagating S-waves: (a) transmitted and reflected S-waves when $A_v = 0.1$ m/s; (b) relative shear displacements and shear stresses for different in situ stresses when $A_v = 0.1$ m/s; (c) transmitted and reflected S-waves when $A_v = -0.1$ m/s; and (d) relative shear displacements and shear stresses for different in situ stresses when $A_v = -0.1$ m/s.

of the shear displacements are SC1–SO–SC2 and SD1–SO–SD2 when $\sigma_{sv} = 0.5$ and 2.5 MPa, respectively. When the joint is subjected to $\sigma_{sv} = 0.5$ MPa and $v = -0.1$ m/s, the transmitted waveform is not cut off; that is, slipping does not occur (in contrast to what happens when $v = 0.1$ m/s). This is because the maximum shear stress of the joint when $v = -0.1$ m/s is 0.43 MPa, which is smaller than the shear strength (0.478 MPa).

Therefore, the propagation of S-waves across an in situ stressed rock mass not only is closely related to the properties of the joints, but also is dependent on the magnitude and direction of the in situ stress. Furthermore, although the initial properties of two joints may be the same, their deformation and transmission of propagating waves both will be different if they are subject to different in situ stresses.

Fig. 7 shows the results obtained when the waves impinge obliquely upon a joint subject to different in situ stress. The angle of incidence used here is 20°, but the other parameters are the same as those in the previous section.

To further investigate the influence of in situ stress, eight coefficients ($T_{\underrightarrow{pp}}$, $T_{\underrightarrow{ps}}$, $T_{\underrightarrow{sp}}$, $T_{\underrightarrow{ss}}$, $R_{\underrightarrow{pp}}$, $R_{\underrightarrow{ps}}$, $R_{\underrightarrow{sp}}$, and $R_{\underrightarrow{ss}}$) are defined according to the following expressions:

$$T_{\underrightarrow{kc}} = \frac{\max(v_{Tc})}{\max(v_{Ik})}, \qquad R_{\underrightarrow{kc}} = \frac{\max(v_{Rc})}{\max(v_{Ik})} \tag{22}$$

where $T_{\underrightarrow{kc}}$ = transmission coefficient; and $R_{\underrightarrow{kc}}$ = reflection coefficient. The subscripts $\underrightarrow{k}$ denote the nature of the incident wave, and the subscript c represents the nature of the transmitted wave ($T_{\underrightarrow{kc}}$) or the reflection wave ($R_{\underrightarrow{kc}}$), where p signifies a P-wave and s signifies an S-wave. Tables 1 and 2 display the values calculated for these coefficients using the data in Fig. 7. As the in situ stress increases, the transmission coefficients (T_{pp}, T_{ps}, T_{sp}, T_{ss}) increase, whereas the reflection coefficients (R_{pp}, R_{ps}, R_{sp}, R_{ss}) decrease, for both P- and S-incident waves. The direction of particle vibration of the incident wave clearly has a significant effect on these reflection and transmission coefficients.

The corresponding joint closures and shear displacements induced by the wave propagation are shown in Figs. 7(b, d, and f). The in situ stress plays an important role in the joint deformation induced by wave propagation. The lower the in situ stress, the greater is the joint closure and shear displacement induced by the stress wave. Slipping occurs when $v = 0.1$ and -0.1 m/s for obliquely incident S-waves, which is different from the behavior found when the S-wave is incident normally. The normal stress changes when the S-wave is incident obliquely, and this determines the shear strength of the joint.

The relationship between stress and displacement induced by the stress wave is more complicated in this case than when the stress wave propagates normally. For the same amplitude of the

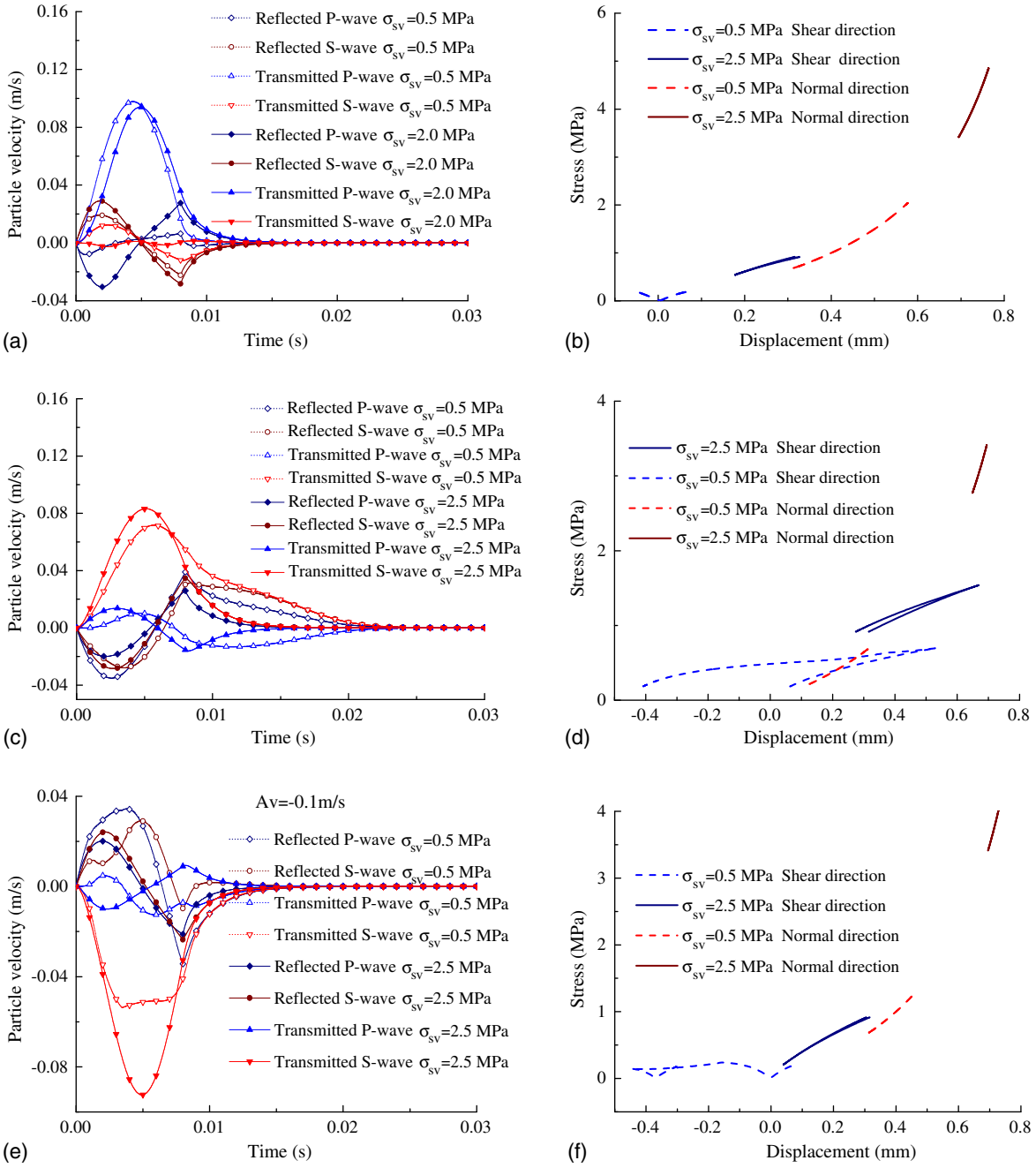

Fig. 7. Effect of in situ stress on the propagation of obliquely incident S- and P-waves: (a) transmitted and reflected waves for incident P-waves; (b) relative shear displacements and closure for different in situ stresses and incident P-waves; (c) transmitted and reflected waves for incident S-waves with $A_v = -0.1$ m/s; (d) relative shear displacements and closure for incident S-waves with $A_v = 0.1$ m/s; (e) transmitted and reflected waves for incident S-waves with $A_v = -0.1$ m/s; and (f) relative shear displacements and closure for incident S-wave with $A_v = -0.1$ m/s.

Table 1. Transmission and reflection coefficients for incident P-waves

In situ stress	T_{pp}	T_{ps}	R_{ps}	R_{pp}
$\sigma_{sv} = 0.5$ MPa	0.94	0.02	0.30	0.30
$\sigma_{sv} = 2.5$ MPa	0.98	0.13	0.23	0.08

Table 2. Transmission and reflection coefficients for incident S-waves

Incident amplitude	In situ stress	T_{sp}	T_{ss}	R_{ss}	R_{sp}
$A_v = 0.1$ m/s	$\sigma_{sv} = 0.5$ MPa	0.13	0.71	0.32	0.38
	$\sigma_{sv} = 2.5$ MPa	0.16	0.83	0.35	0.26
$A_v = -0.1$ m/s	$\sigma_{sv} = 0.5$ MPa	0.11	0.54	0.29	0.34
	$\sigma_{sv} = 2.5$ MPa	0.10	0.92	0.25	0.22

incident S-wave ($A_v = -0.1$ m/s) and same in situ stress ($\sigma_{sv} = 0.5$ MPa), the transmitted S-wave is cut off if incidence is oblique, whereas this does not occur for normal incidence. The results thus demonstrate that the wave attenuation and joint displacement both are affected by the angle of incidence and joint angle.

Parametric Studies

To investigate wave propagation across a stressed joint, parametric studies were carried out. To simplify the following analyses, two

additional coefficients were defined: T_e is the energy transmission coefficient, and R_e is the energy reflection coefficient. These can be calculated using the expressions

$$E_{\text{inc}} = z\int_0^{tn} v_{\text{inc}}^2(t)dt = z_p\sum_{i=1}^{n} v_{\text{inc}}^2(t_i)\Delta t$$

$$E_{\text{tra},p} = z_p\sum_{i=1}^{n} v_{\text{tra},p}^2(t_i)\Delta t; \qquad E_{\text{tra},s} = z_s\sum_{i=1}^{n} v_{\text{tra},s}^2(t_i)\Delta t$$

$$E_{\text{ref},p} = z_p\sum_{i=1}^{n} v_{\text{ref},p}^2(t_i)\Delta t; \qquad E_{\text{ref},s} = z_s\sum_{i=1}^{n} v_{\text{ref},s}^2(t_i)\Delta t \tag{23}$$

$$T_e = \frac{E_{\text{tra},p} + E_{\text{tra},s}}{E_{\text{inc}}}$$

$$R_e = \frac{E_{\text{ref},p} + E_{\text{ref},s}}{E_{\text{inc}}} \tag{24}$$

where $E_{\text{tra},p}$ ($E_{\text{ref},p}$) and $E_{\text{tra},s}$ ($E_{\text{ref},s}$) = energies of the transmitted (reflected) P- and S-waves, respectively; and E_{inc} = energy of the incident wave.

Effects of In Situ Stress and Lateral Pressure Coefficient

Fig. 8 illustrates the influence of the in situ stress on T_e and R_e. Half-cycle P- and S-waves were used in this analysis. The amplitude of incidence and frequency of the incident waves were 0.1 m/s and 50 Hz, respectively. The joint angle and the angle of incidence and were set to 30° and 10°, respectively. The initial normal stiffness (k_{ni}) was taken as 3.2 GPa/m, and $d_{\max} = 1$ mm. The initial shear stiffness number (K_j) was 3.88 GPa/m. The stiffness exponent (n_i) and failure ratio (R_f) were 0.000725 and 0.810, respectively, which are the typical values for weathered sandstone (Bandis et al. 1983; Kulhawy 1975). The in situ gravitational stress varied from 0.2 to 16 MPa, and the lateral pressure coefficient (k_v) varied from 0.5 to 2 (in increments of 0.5).

Fig. 8(a) shows the results for incident P-waves; T_e increases nonlinearly, and R_e decreases nonlinearly, as the gravitational stress σ_{sv} increases. The slopes of both sets of curves (T_e and R_e) decrease in magnitude as σ_v increases. After σ_v reaches 4 MPa, the values of T_e and R_e remain approximately constant. This is because the joint effectively becomes welded if the in situ stress is sufficiently large (Fan and Sun 2015).

Fig. 8(b) shows the case of S-wave propagation with $A_v = 0.1$ m/s. For $k_v \le 1$, T_e first increases rapidly as the in situ stress increases and then increases much more slowly as it asymptotically approaches a constant value; correspondingly, R_e first decreases rapidly and then more slowly as it approaches a constant value. When $k_v = 1.5$, T_e increases linearly and R_e fluctuates when the gravitational stress increases from 0 to 1 MPa. As the gravitational stress increases, T_e increases slightly to a constant value (about 0.68) and R_e decreases slightly to a constant value (about 0.32). When $k_v = 2$, T_e increases linearly and R_e deceases at first and then increases as the gravitational stress increases from 0 to 6 MPa. As the in situ stress increases further, T_e increase slightly to a constant value (about 0.43) and R_e decreases slightly to a constant value (about 0.58). In addition, increasing the k_v value results in a decrease in T_e and an increase in R_e.

Fig. 8(c) shows the results for S-wave propagation with $A_v = -0.1$ m/s. When $k_v \le 1$, with the in situ stress increasing, T_e and R_e change in a way that is similar to the variation found when $A_v = 0.1$ m/s. When $k_v > 1$, T_e increases rapidly at first and then falls to a constant value (0.70 for $k_v = 1.5$ and 0.41

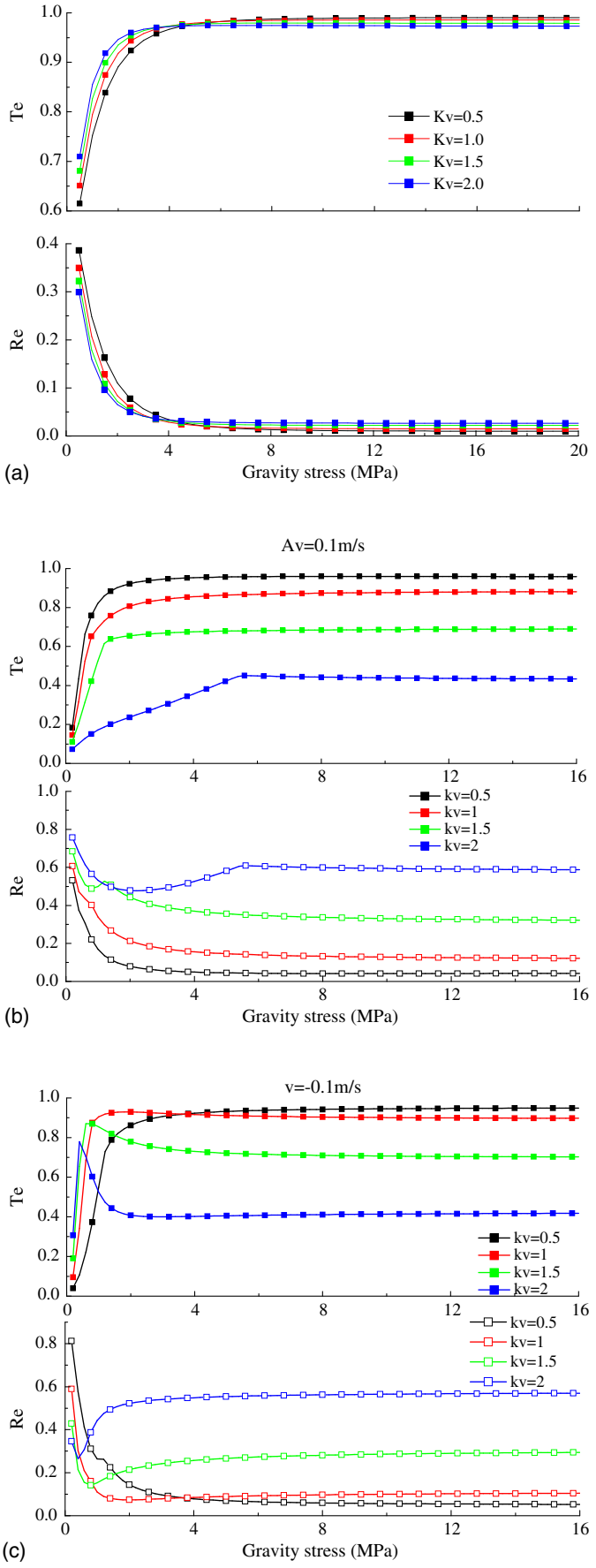

Fig. 8. Effect of in-situ stress on transmission coefficients T_e and reflection coefficients R_e: (a) P-wave; (b) S-wave with $A_v = 0.1$ m/s; and (c) S-wave with $A_v = -0.1$ m/s.

for $k_v = 2$). At the same time, R_e decreases rapidly at first and then gradually rises to a constant value (0.29 for $k_v = 1.5$ and 0.47 for $k_v = 2$).

These results confirm that the in situ stress and lateral pressure coefficient have a significant effect on wave propagation across the joint. The wave propagation is controlled by the combined effect of the stress wave and in situ stress. The direction of shear stress τ_w induced by the dynamic stress wave may not be consistent with that of the initial shear stress τ_s caused by the in situ stress. When the direction of τ_w is the same as that of τ_s, the combined effect of shear stress on the joint becomes larger and the joint is more likely to slip. When the direction of τ_w is different from that of τ_s, the displacement caused by the stress wave counteracts the displacement caused by the initial displacement (which can be considered to correspond to unloading), and deformation can occur in the opposite direction to the initial shear displacement.

When the in situ stress is sufficiently large, its effect on the wave attenuation can be neglected. This agrees with the conclusions drawn by Cui et al. (2017) and Fan and Sun (2015). The greater the in situ stress, the greater are the shear strength, shear stiffness, and normal stiffness. As a result, more energy is transmitted through the joint, which reduces the likelihood that the joint will fail.

Effect of Angle of Incidence

The effect of angle of incidence on wave propagation has been systemically studied for incident P-waves using a linear model (Li et al. 2012; Zhao et al. 2006) and the B-B model (Li 2013). This section focuses mainly on waves propagating obliquely across an in situ stressed joint using three different joint deformation models, the parameters of which are given in section "Special Case and Comparison."

Fig. 9 shows how the transmission and reflection coefficients vary for P- and S-waves as a function of their angle of incidence for the three different joint models. Clearly, the varying effect of the incidence angle differs depending on the joint model used. For P-waves [Fig. 9(a)] and using the linear joint model, T_e gently increases as α increases from 0° to 40°, and R_e gently decreases. However, with further increases in α, from 40° to 75°, T_e increases substantially to about 0.81, and R_e decreases substantially to 0.05.

For the nonlinear joint models, two critical angles (α_A and α_B) divide the pattern of behavior into three parts [Fig. 9(a)]. When $\alpha \le \alpha_A$, T_e decreases and R_e increases as α increases. When $\alpha_A < \alpha \le \alpha_B$, this variation is reversed, and T_e increases and R_e decreases as α increases. Finally, as α is increased beyond α_B and approaches 90°, T_e decreases dramatically and R_e increases dramatically. For the Nonlinear 1 model $\alpha_A \sim 50°$, and for the Nonlinear 2 $\alpha_A \sim 35°$; the corresponding values of α_B are both ~80°.

Let T_{e0} and R_{e0} represent the values of the coefficients when the P-wave is incident normally, and define T_{ev} as the ratio of the maximum change ΔT_e to T_{e0}, where ΔT_e is the change in Re value, i.e., $\Delta T_{ev} = |T_e - T_{e0}|$ [similarly, $R_{ev} = \max(\Delta R_e/R_{e0})$]. As α increases from 0° to 90°, T_{ev} and R_{ev} are ~28% and ~86% for the linear model, respectively. The corresponding figures for the Nonlinear 1 model are ~11% and ~140%, and for the Nonlinear 2 model they are ~5% and ~85%. Thus, compared with the other two joint models, the Nonlinear 2 model is much less sensitive to angular variation.

Fig. 9(b) shows the effect of varying the angle of incidence of S-waves (β) on the reflection and transmission energy coefficients for the different joint models. Here, the value of β varies from 0° to the critical angle 36°, as suggested by Li et al. (2012). The curves produced using the three models are significantly different, especially for the reflection coefficients.

For the linear model, increasing the angle of incidence leads to an increase in both the transmitted and reflected energy. For the two nonlinear models, T_e increases and R_e decreases as the incident angle increases for both $A_v = 0.1$ and -0.1 m/s. This is because the shear strength of the nonlinear joint models is dependent on the normal stress, which is related to the angle of incidence. Therefore, the nonlinear model has considerable merit when calculating the effect of the energy dissipation. It also is apparent that the Nonlinear 2 model is more sensitive to the direction of the particle vibration than is the Nonlinear 1 model.

Effect of Amplitude of Incident Wave

Fig. 10 shows the effect on the energy coefficients of varying the incident wave amplitude for the three different joint models. The other parameters used in this case are the same as those used in section "Effect of Angle of Incidence." It is immediately obvious that the reflection and transmission energy coefficients for P- and S-waves propagating across a linear joint remain

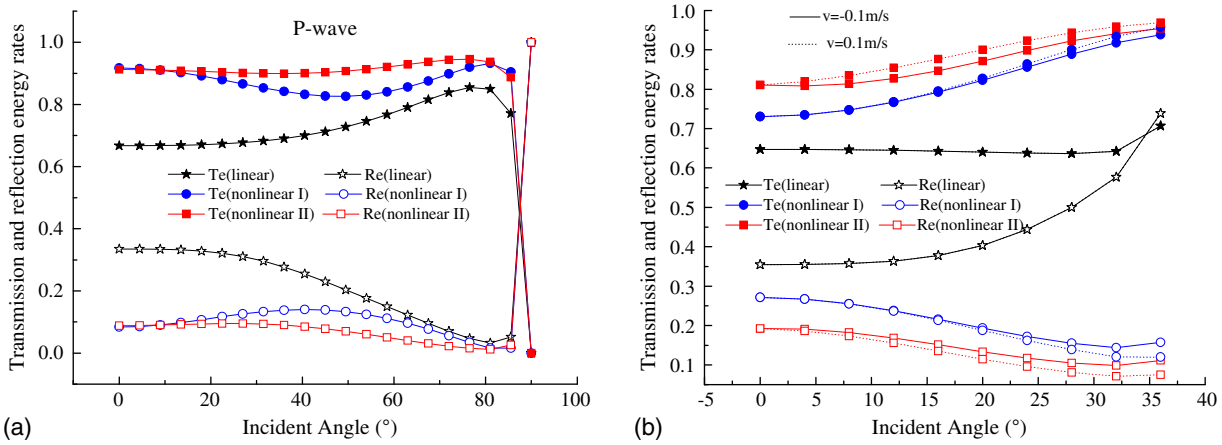

Fig. 9. Variation of the energy coefficients T_e and R_e as a function of the angle of incidence of the incident wave for different joint models when the incident waves are (a) P-waves; and (b) S-waves.

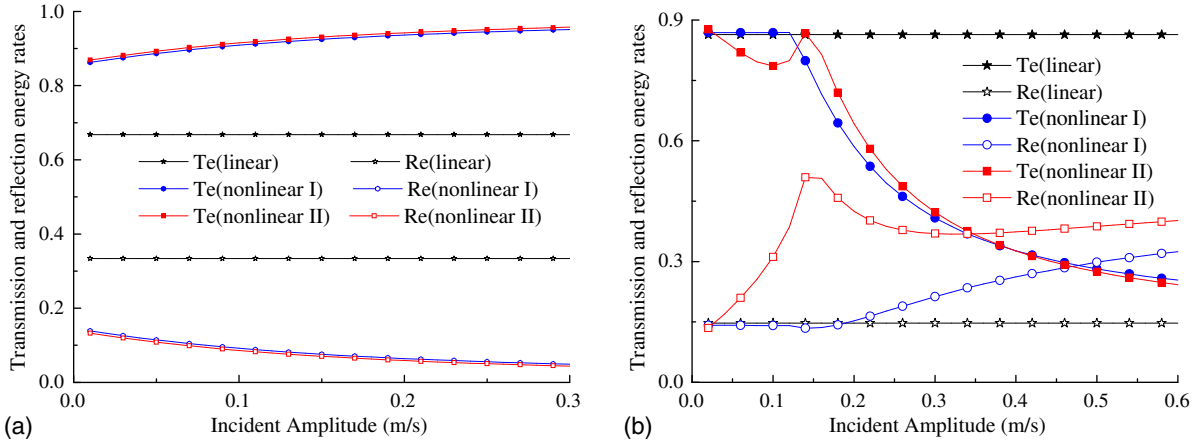

Fig. 10. Variation of the energy coefficients T_e and R_e as a function of the amplitude of the incident wave for different joint models when the incident waves are (a) P-waves; and (b) S-waves.

constant irrespective of the incident wave amplitude. This is because the stiffness and strength of the linear joint are independent of the stress and remain unchanged as the wave propagates. However, when P-waves are incident on either of the nonlinear joint models [Fig. 10(a)], moderate increases in T_e and decreases in R_e occur as the incident amplitude is increased. In fact, T_e in the Nonlinear 2 joint model is slightly larger than that obtained using the Nonlinear 1 joint model. This is because the shear stiffness of the Nonlinear 2 model depends on both the normal and shear stress during wave propagation.

When S-waves are incident on the Nonlinear 1 joint model [Fig. 10(b)], T_e and R_e barely change when the incident amplitude is kept below 0.12 m/s. This is because the shear stiffness stays the same before the joint slips. Increasing the incident amplitude beyond this value causes T_e to decrease sharply because energy is dissipated when slipping occurs.

The behavior of S-waves incident on a joint described using the Nonlinear 2 model is more complicated [Fig. 10(b)]. As the incident amplitude increases from 0.02 to 0.14 m/s, R_e increases dramatically, whereas T_e decreases at first and then recovers somewhat. As the incident amplitude continues to increase, both T_e and R_e decrease significantly, indicating that there is considerable dissipation of the energy. The normal stiffness increases with increasing normal stress, and the shear stiffness is affected by both the normal and shear stress. Therefore, the variation of the transmitted and reflected energy is a result of the combined effect of varying normal and shear stiffness.

When a wave propagates across a joint, the deformation and damage of the joint causes dissipation and absorption of stress wave energy. To compare the relationship between the energy absorption of the stress wave and the incident wave amplitude under different joint models, two parameters, energy absorption coefficient e_{ab}, and transmission and reflection of incident energy coefficient e_{tar}, are defined in Eq. (25), which is based on Eq. (23)

$$e_{\text{tar}} = \frac{E_{\text{tra},p} + E_{\text{tra},s} + E_{\text{ref},p} + E_{\text{ref},s}}{E_{\text{inc}}} = T_e + R_e$$
$$e_{ab} = 1 - e_{\text{tar}} \tag{25}$$

where $E_{\text{tra},p}$ ($E_{\text{ref},p}$) and $E_{\text{tra},s}$ ($E_{\text{ref},s}$) = energies of transmitted (reflected) P- and S-waves, respectively; and E_{inc} = energy of the incident wave.

The relationships between e_{ab} and e_{tar} and the amplitude of the incident wave are different (Fig. 11).

The shear strength and stiffness of the joint for Nonlinear 1 model remain unchanged when it is not destroyed. Therefore, the amount of energy absorbed by joint is constant (albeit small). When the shear stress of the joint exceeds the shear strength, the joint is destroyed, and more wave energy is absorbed. For the Nonlinear 2 model, the large amount of wave energy also is absorbed by the joint for an incident S-wave of large amplitude. The direction of vibration of the incident S-wave is important in the Nonlinear 2 model. When the S-wave has a positive amplitude, which means that the direction of deformation caused by the S-wave is the same as that of the initial shear deformation caused by the in situ shear stress, the value of e_{ab} first decreases and then increases. The negative value of e_{ab} denotes a release of in situ stress. Under dynamic disturbance, the energy associated with the in situ stress also may be released, so the sum of the energy in the reflected and transmitted waves is greater than the incident energy of the stress wave. The wave absorption of the joint increases rapidly after joint slip; this explains why a small dynamic disturbance generates a relatively large geological hazard. The comparison of

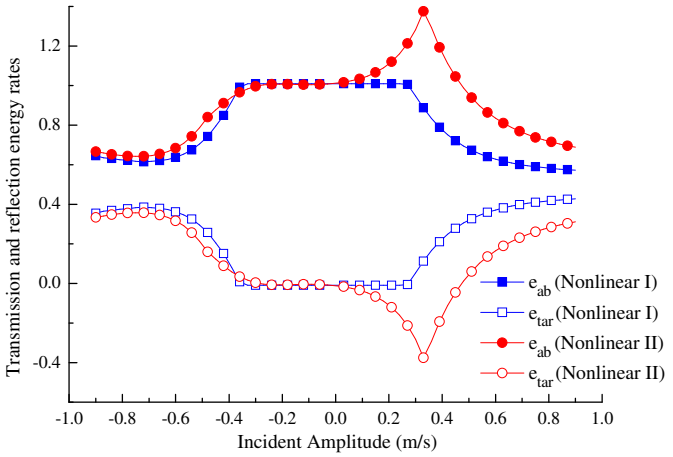

Fig. 11. Variation of the energy absorption coefficients e_{ab} and e_{tar} as a function of the amplitude of the incident wave for different joint models (incident S-waves, $\sigma_{sv} = 3.0$ MPa).

the two models shows that the effect of in situ stress on stress wave propagation can be better considered by the Nonlinear joint 2 model.

Conclusions

This study extended the TDRM to investigate seismic wave propagation through a joint in an in situ stressed rock mass. The gravitational and tectonic stress and dip angle of the joint were used to calculate the initial stresses in normal and tangential directions. The B-B model and hyperbolic nonlinear slip model were used to investigate of the effect of the joint on waves propagating obliquely across the jointed rock mass.

A comparison of the HN model and previous joint models (linear and Coulomb slip models) showed that the HN model depends on the stress history and shear stiffness degradation. Extensive parametric analyses subsequently were conducted to study the effect of gravitational stress, lateral pressure coefficient, and amplitude and angle of incidence of the seismic wave. Compared with the other two models, the HN model is less sensitive to the angle of incidence but is more dependent upon the incident wave amplitude.

This study showed that the combined influence of in situ stress and dynamic stress is complicated and affects the dynamic displacement of the joint induced by wave propagation. The effect of the in situ stress on wave attenuation depends not only on the gravitational and tectonic stress but also on the direction of the particle vibration of the incident wave. The deformation of the joint and the probability that failure will occur because of the stress induced by waves of identical amplitude therefore may be different even if the value of the in situ stress is the same. That is, the behavior of the joint depends on whether or not the direction of the initial shear stress is consistent with the direction of wave propagation.

A simplified waveform (half-sine) was used for the incident wave in this work to study the combined effect of dynamic and in situ stresses. More-complicated waveforms, e.g., those of real seismic waves and blast waves, need to be studied in future work. In addition, the rock in the present study was simulated using a linear model. Therefore, nonlinear rock materials and rock masses featuring more joints also need to be investigated further.

Data Availability Statement

Some or all data, models, or code generated or used during the study are available from the corresponding author by request, including the original data for Figs. 3–11.

Acknowledgments

The research was financially supported by the National Natural Science Foundation of China (Grant Nos. 51609183 and 51774222); the Natural Science Foundation of Hubei Province, China (Grant No. 2017CFB508); the Open Research Fund of the State Key Laboratory of Geomechanics and Geotechnical Engineering, Institute of Rock and Soil Mechanics, Chinese Academy of Sciences (Nos. Z015005 and Z018009); and the project supported by the Hubei Key Laboratory of Roadway Bridge and Structure Engineering (Wuhan University of Technology) (DQJJ201710).

References

Aydan, Ö., Y. Ohta, M. Geniş, and K. Ohkubo. 2010. "Response and stability of underground structures in rock mass during earthquakes." *Rock Mech. Rock Eng.* 43 (6): 857–875. https://doi.org/10.1007/s00603-010-0105-6.

Bandis, S. C., A. C. Lumsden, and N. R. Barton. 1983. "Fundamentals of rock joint deformation." *Int. J. Rock Mech. Min. Sci.* 20 (6): 249–268. https://doi.org/10.1016/0148-9062(83)90595-8.

Barton, N. 1976. "The shear strength of rock and rock joints." *Int. J. Rock Mech. Min. Sci.* 13 (9): 255–279. https://doi.org/10.1016/0148-9062(76)90003-6.

Biot, M. A. 1963. "Theory of stability and consolidation of a porous medium under initial stress." *J. Math. Mech.* 12 (2): 521–541. https://doi.org/10.1512/iumj.1963.12.12033.

Brown, E. T., and E. Hoek. 1978. "Trends in relationships between measured in-situ stresses and depth." *Int. J. Rock Mech. Min. Sci.* 15 (4): 211–215. https://doi.org/10.1016/0148-9062(78)91227-5.

Chen, X., and Z. Xu. 2016. "The ultrasonic P-wave velocity-stress relationship of rocks and its application." *Bull. Eng. Geol. Environ.* 76 (2): 1–9. https://doi.org/10.1007/s10064-016-0866-6.

Cheng, G. W., T. H. Ma, C. A. Tang, H. Y. Liu, and S. J. Wang. 2017. "A zoning model for coal mining - induced strata movement based on microseismic monitoring." *Int. J. Rock. Mech. Min. Sci.* 94 (Apr): 123–138. https://doi.org/10.1016/j.ijrmms.2017.03.001.

Cook, N. G. W. 1992. "Natural joints in rock: Mechanical, hydraulic and seismic behaviour and properties under normal stress." *Int. J. Rock Mech. Min. Sci.* 29 (3): 198–223. https://doi.org/10.1016/0148-9062(92)93656-5.

Cui, Z., Q. Sheng, and X. L. Leng. 2017. "Analysis of S wave propagation through a nonlinear joint with the continuously yielding model." *Rock Mech. Rock Eng.* 50 (1): 113–123. https://doi.org/10.1007/s00603-016-1108-8.

Fairhurst, C. 2003. "Stress estimation in rock: A brief history and review." *Int. J. Rock Mech. Min. Sci.* 40 (7–8): 957–973. https://doi.org/10.1016/j.ijrmms.2003.07.002.

Fan, L. F., and H. Y. Sun. 2015. "Seismic wave propagation through an in-situ stressed rock mass." *J. Appl. Geophys.* 121 (Oct): 13–20. https://doi.org/10.1016/j.jappgeo.2015.07.002.

Fuchs, K., and B. Müller. 2001. "World stress map of the earth: A key to tectonic processes and technological applications." *Naturwissenschaften* 88 (9): 357–371. https://doi.org/10.1007/s001140100253.

Guz, A. N. 2002. "Elastic waves in bodies with initial (residual) stresses." *Int. Appl. Mech.* 38 (1): 23–59. https://doi.org/10.1023/A:1015379824503.

Hoek, E. 1983. "Strength of jointed rock masses." *Géotechnique* 33 (3): 187–223. https://doi.org/10.1680/geot.1983.33.3.187.

Kahraman, S. 2001. "Evaluation of simple methods for assessing the uniaxial compressive strength of rock." *Int. J. Rock Mech. Min. Sci.* 38 (7): 981–994. https://doi.org/10.1016/S1365-1609(01)00039-9.

Korinets, A., and H. Alehossein. 2002. "Technical note on the initial non-linearity of compressive stress-strain curves for intact rock." *Rock Mech. Rock Eng.* 35 (4): 319–328. https://doi.org/10.1007/s00603-002-0030-4.

Kulhawy, F. H. 1975. "Stress deformation properties of rock and rock discontinuities." *Eng. Geol.* 9 (4): 327–350. https://doi.org/10.1016/0013-7952(75)90014-9.

Kumar, S. A., M. K. Ch, and A. Chattopadhyay. 2015. "Love-type wave propagation in an irregular prestressed composite sandwiched layer." *Int. J. Geomech.* 16 (2): 04015060. https://doi.org/10.1061/(ASCE)GM.1943-5622.0000536.

Li, J. C. 2013. "Wave propagation across non-linear rock joints based on time-domain recursive method." *Geophys. J. Int.* 193 (2): 970–985. https://doi.org/10.1093/gji/ggt020.

Li, J. C., H. B. Li, G. W. Ma, and J. Zhao. 2012. "A time-domain recursive method to analyze transient wave propagation across rock joints." *Geophys. J. Int.* 188 (2): 631–644. https://doi.org/10.1111/j.1365-246X.2011.05286.x.

Li, J. C., H. B. Li, and J. Zhao. 2015. "An improved equivalent viscoelastic medium method for wave propagation across layered rock masses."

Int. J. Rock Mech. Min. Sci. 73 (1): 62–69. https://doi.org/10.1016/j.ijrmms.2014.10.008.

Liu, E., J. A. Hudson, and T. Pointer. 2000. "Equivalent medium representation of fractured rock." *J. Geophys. Res.* 105 (B2): 2981. https://doi.org/10.1029/1999JB900306.

Meng, F. Z., L. N. Y. Wong, H. Zhou, and Z. Q. Wang. 2018. "Comparative study on dynamic shear behavior and failure mechanism of two types of granite joint." *Eng. Geol.* 245 (1): 356–369. https://doi.org/10.1016/j.enggeo.2018.09.005.

Meng, F. Z., L. N. Y. Wong, H. Zhou, J. Yu, and G. T. Cheng. 2019. "Shear rate effects on the post-peak shear behaviour and acoustic emission characteristics of artificially split granite joints." *Rock Mech. Rock Eng.* 52 (7): 2155–2174. https://doi.org/10.1007/s00603-018-1722-8.

Misra, A., and O. Marangos. 2010. "Rock-joint micromechanics: Relationship of roughness to closure and wave propagation." *Int. J. Geomech.* 11 (6): 431–439. https://doi.org/10.1061/(ASCE)GM.1943-5622.0000021.

Mohd-Nordin, M. M., K. I. Song, G. C. Cho, and Z. Mohamed. 2014. "Long-wavelength elastic wave propagation across naturally fractured rock masses." *Rock Mech. Rock Eng.* 47 (2): 561–573. https://doi.org/10.1007/s00603-013-0448-x.

Ning, Y., J. Yang, G. W. Ma, and P. Chen. 2011. "Modelling rock blasting considering explosion gas penetration using discontinuous deformation analysis." *Rock Mech. Rock Eng.* 44 (4): 483–490. https://doi.org/10.1007/s00603-010-0132-3.

Pappalardo, G. 2015. "Correlation between P-wave velocity and physical–mechanical properties of intensely jointed dolostones, Peloritani Mounts, NE Sicily." *Rock Mech. Rock Eng.* 48 (4): 1711–1721. https://doi.org/10.1007/s00603-014-0607-8.

Pestman, B. J., and J. G. V. Munster. 1996. "An acoustic emission study of damage development and stress-memory effects in sandstone." *Int. J. Rock. Mech. Min. Sci.* 33 (6): 585–593. https://doi.org/10.1016/0148-9062(96)00011-3.

Pyrak-Nolte, L. J., L. R. Myer, and N. G. W. Cook. 1990. "Transmission of seismic waves across single natural fractures." *J. Geophys. Res.* 95 (B6): 8617–8638. https://doi.org/10.1029/JB095iB06p08617.

Sebastian, R., and T. G. Sitharam. 2016. "Transformations of obliquely striking waves at a rock joint: Numerical simulations." *Int. J. Geomech.* 16 (3): 04015079. https://doi.org/10.1061/(ASCE)GM.1943-5622.0000575.

Selim, M. M., and M. K. Ahmed. 2006. "Propagation and attenuation of seismic body waves in dissipative medium under initial and couple stresses." *Appl. Math. Comput.* 182 (2): 1064–1074. https://doi.org/10.1016/j.amc.2006.05.005.

Shams, M. 2016. "Effect of initial stress on love wave propagation at the boundary between a layer and a half-space." *Wave Motion* 65 (Sep): 92–104. https://doi.org/10.1016/j.wavemoti.2016.04.009.

Sharma, M. D. 2005. "Effect of initial stress on the propagation of plane waves in a general anisotropic poroelastic medium." *J. Geophys. Res.-Solid Earth* 110 (B11): 1–14. https://doi.org/10.1029/2005JB003779.

Singh, A. K., A. Das, A. Chattopadhyay, and S. Dhua. 2015. "Dispersion of shear wave propagating in vertically heterogeneous double layers overlying an initially stressed isotropic half-space." *Soil Dyn. Earthquake Eng.* 69 (Feb): 16–27. https://doi.org/10.1016/j.soildyn.2014.10.021.

Tolstoy, I. 1982. "On elastic waves in prestressed solids." *J. Geophys. Res.-Solid Earth* 87 (B8): 6823–6827. https://doi.org/10.1029/JB087iB08p06823.

Utagawa, M., M. Seto, and K. Katsuyama. 1997. "Estimation of initial stress by deformation rate analysis (DRA)" *Int. J. Rock. Mech. Min. Sci.* 34 (3–4): 501. https://doi.org/10.1016/S1365-1609(97)00095-6.

Yasar, E., and Y. Erdogan. 2004. "Correlating sound velocity with the density, compressive strength and young's modulus of carbonate rocks." *Int. J. Rock. Mech. Min. Sci.* 41 (5): 871–875. https://doi.org/10.1016/j.ijrmms.2004.01.012.

Zhang, L. 2010. "Estimating the strength of jointed rock masses." *Rock Mech. Rock Eng.* 43 (4): 391–402. https://doi.org/10.1007/s00603-009-0065-x.

Zhao, J., and J. G. Cai. 2001. "Transmission of elastic p-waves across single fractures with a nonlinear normal deformational behavior." *Rock Mech. Rock Eng.* 34 (1): 3–22. https://doi.org/10.1007/s006030170023.

Zhao, J., J. G. Cai, X. B. Zhao, and H. B. Li. 2008. "Dynamic model of fracture normal behaviour and application to prediction of stress wave attenuation across fractures." *Rock Mech. Rock Eng.* 41 (5): 671–693. https://doi.org/10.1007/s00603-006-0127-2.

Zhao, J., X. B. Zhao, and J. G. Cai. 2006. "A further study of P-wave attenuation across parallel fractures with linear deformational behaviour." *Int. J. Rock. Mech. Min. Sci.* 43 (5): 776–788. https://doi.org/10.1016/j.ijrmms.2005.12.007.

Zhao, X. B., J. B. Zhu, J. Zhao, and J. G. Cai. 2012. "Study of wave attenuation across parallel fractures using propagator matrix method." *Int. J. Numer. Anal. Methods Geomech.* 36 (10): 1264–1279. https://doi.org/10.1002/nag.1050.

Zhou, X., L. Fan, and Z. Wu. 2017. "Effects of microfracture on wave propagation through rock mass." *Int. J. Geomech.* 17 (9): 04017072. https://doi.org/10.1061/(ASCE)GM.1943-5622.0000947.

Zhu, J. B., A. Perino, G. F. Zhao, G. Barla, J. C. Li, G. W. Ma, and J. Zhao. 2011. "Seismic response of a single and a set of filled joints of viscoelastic deformational behaviour." *Geophys. J. Int.* 186 (3): 1315–1330. https://doi.org/10.1111/j.1365-246X.2011.05110.x.